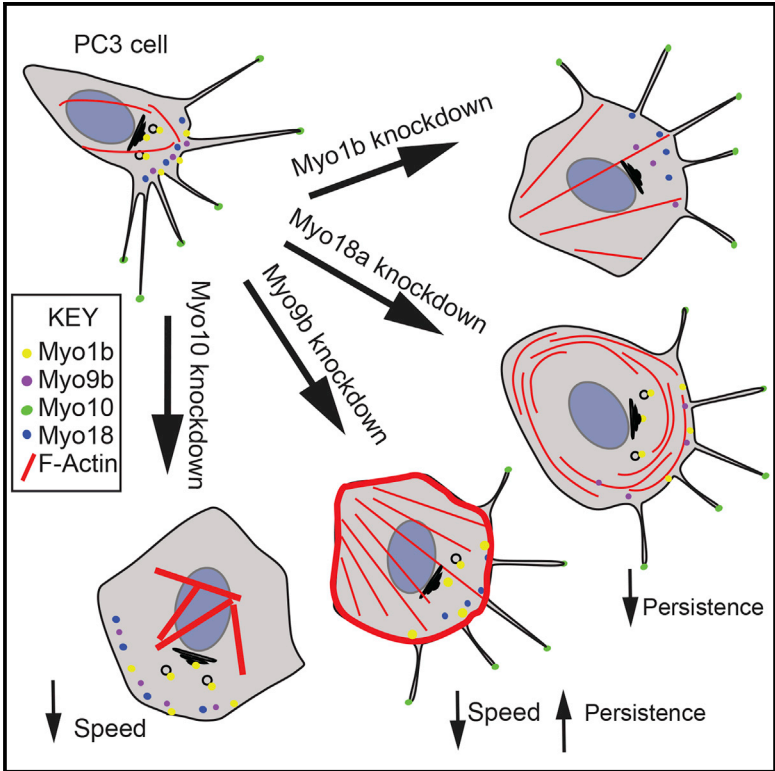# Cell Reports

Specific Myosins Control Actin Organization, Cell Morphology, and Migration in Prostate Cancer Cells

Graphical Abstract

Authors

Katarzyna A. Makowska, Ruth E. Hughes, Kathryn J. White, Claire M. Wells, Michelle Peckham

Correspondence

claire.wells@kcl.ac.uk (C.M.W.),
m.peckham@leeds.ac.uk (M.P.)

In Brief

Makowska et al. show that several myosin isoforms (Myo1b, Myo9b, Myo10, and Myo18a) are overexpressed in metastatic prostate cancer. Knockdown of each of the myosins resulted in distinct cell phenotypes, showing that they can contribute to metastasis through re-organization of the actin cytoskeleton in addition to motor activity.

Highlights

- Myo1b, Myo9b, Myo10, and Myo18a are highly expressed in metastatic prostate cancer

- Knockdown of individual myosins distinctly affects the cytoskeleton and cell migration

- Myosins act in concert to directly influence actin organization and cell migration

- Misregulation of myosin expression may drive the metastatic phenotype

Specific Myosins Control Actin Organization, Cell Morphology, and Migration in Prostate Cancer Cells

Katarzyna A. Makowska,[1] Ruth E. Hughes,[1] Kathryn J. White,[1] Claire M. Wells,[2,*] and Michelle Peckham[1,*]
[1]School of Molecular and Cellular Biology, Faculty of Biological Sciences, University of Leeds, Leeds LS2 9JT, UK
[2]Division of Cancer Studies, King's College London, London SE1 1UL, UK
*Correspondence: claire.wells@kcl.ac.uk (C.M.W.), m.peckham@leeds.ac.uk (M.P.)
 http://dx.doi.org/10.1016/j.celrep.2015.11.012
This is an open access article under the CC BY license (http://creativecommons.org/licenses/by/4.0/).

SUMMARY

We investigated the myosin expression profile in prostate cancer cell lines and found that Myo1b, Myo9b, Myo10, and Myo18a were expressed at higher levels in cells with high metastatic potential. Moreover, Myo1b and Myo10 were expressed at higher levels in metastatic tumors. Using an siRNA-based approach, we found that knockdown of each myosin resulted in distinct phenotypes. Myo10 knockdown ablated filopodia and decreased 2D migration speed. Myo18a knockdown increased circumferential non-muscle myosin 2A-associated actin filament arrays in the lamella and reduced directional persistence of 2D migration. Myo9b knockdown increased stress fiber formation, decreased 2D migration speed, and increased directional persistence. Conversely, Myo1b knockdown increased numbers of stress fibers but did not affect 2D migration. In all cases, the cell spread area was increased and 3D migration potential was decreased. Therefore, myosins not only act as molecular motors but also directly influence actin organization and cell morphology, which can contribute to the metastatic phenotype.

INTRODUCTION

Myosins are a large and diverse family of molecular motors important for cell migration and motility. The human genome encodes 39 myosin genes, subdivided into 12 different classes (Berg et al., 2001; Peckham and Knight, 2009). Class 2 is the largest (13 genes). Ten of these are found exclusively in muscle. The remaining three encode the non-muscle (NM) myosin isoforms 2A, 2B, and 2C, which contribute to cell shape, adhesion, and cytokinesis (Mogilner and Keren, 2009; Vicente-Manzanares et al., 2009). Myosin isoforms in the remaining classes contribute to a wide range of functions, including organelle trafficking, membrane tethering, Golgi organization, actin organization, and actin polymerization (Hartman and Spudich, 2012). Individual cell types only express a subset of myosin genes. Early studies have shown that ~8–11 different myosin isoforms are co-expressed in epithelial cell lines, leukocytes, liver cells, and myoblasts (Bement et al., 1994; Wells et al., 1997). Some myosin isoforms are expressed widely, whereas others (e.g., Myo7a and Myo3) are restricted to a small tissue subset (Dosé and Burnside, 2000; Hasson et al., 1995).

It has never been determined how variation in myosin expression profile between closely related cell types contributes to a variation in cellular phenotype. Modulating myosin expression could help to drive a cell toward a more migratory phenotype and, therefore, metastasis in cancer. Here we determined the myosin isoform expression profile in a range of prostate cell lines and in silico and then investigated four of the overexpressed myosin isoforms to uncover how each contribute to the more highly metastatic phenotype of PC-3 cells (Pulukuri et al., 2005).

RESULTS

Myo1b, Myo9b, Myo10, and Myo18a Are Overexpressed in More Highly Metastatic Cells

We analyzed myosin expression for all 26 of the non-muscle myosin genes in the three most widely used prostate cancer cell lines: PC-3, DU145, and LNCaP (Weber et al., 2004). PC-3 cells are considered to have a higher metastatic potential than LNCaP cells (Aalinkeel et al., 2004). Class 2 muscle myosin isoforms were excluded because they are not expressed in non-muscle cells. We also analyzed a matched pair of normal (1535NP) and cancerous (1535CT) cell lines derived from the prostate of the same patient (Bright et al., 1997).

A core of 12 myosin genes were expressed in all cell lines tested, as demonstrated by RT-PCR (Table S1). However, DU145 cells additionally expressed two myosin isoforms, Myo7a and Myo3, normally only expressed in the cochlea, retina, testis, lung, and kidney (Hasson et al., 1995) or in the retina and pancreas (Dosé and Burnside, 2000) respectively, and, therefore, we did not use these cells in further experiments, although, for completeness, the qPCR analysis on these cells is included (Figure S1).

Expression levels of *MYO1B*, *MYO1D*, *MYO1E*, *MYO9B*, *MYO10*, and *MYO18A* were significantly higher in PC-3 than in LNCaP cells by qPCR (Figure 1A). *MYO1B* and *MYO10* expression levels were also significantly higher in 1535CT than in 1535NP cells (Figure 1B). An in silico analysis (Figure 1C) showed that *MYO1B*,
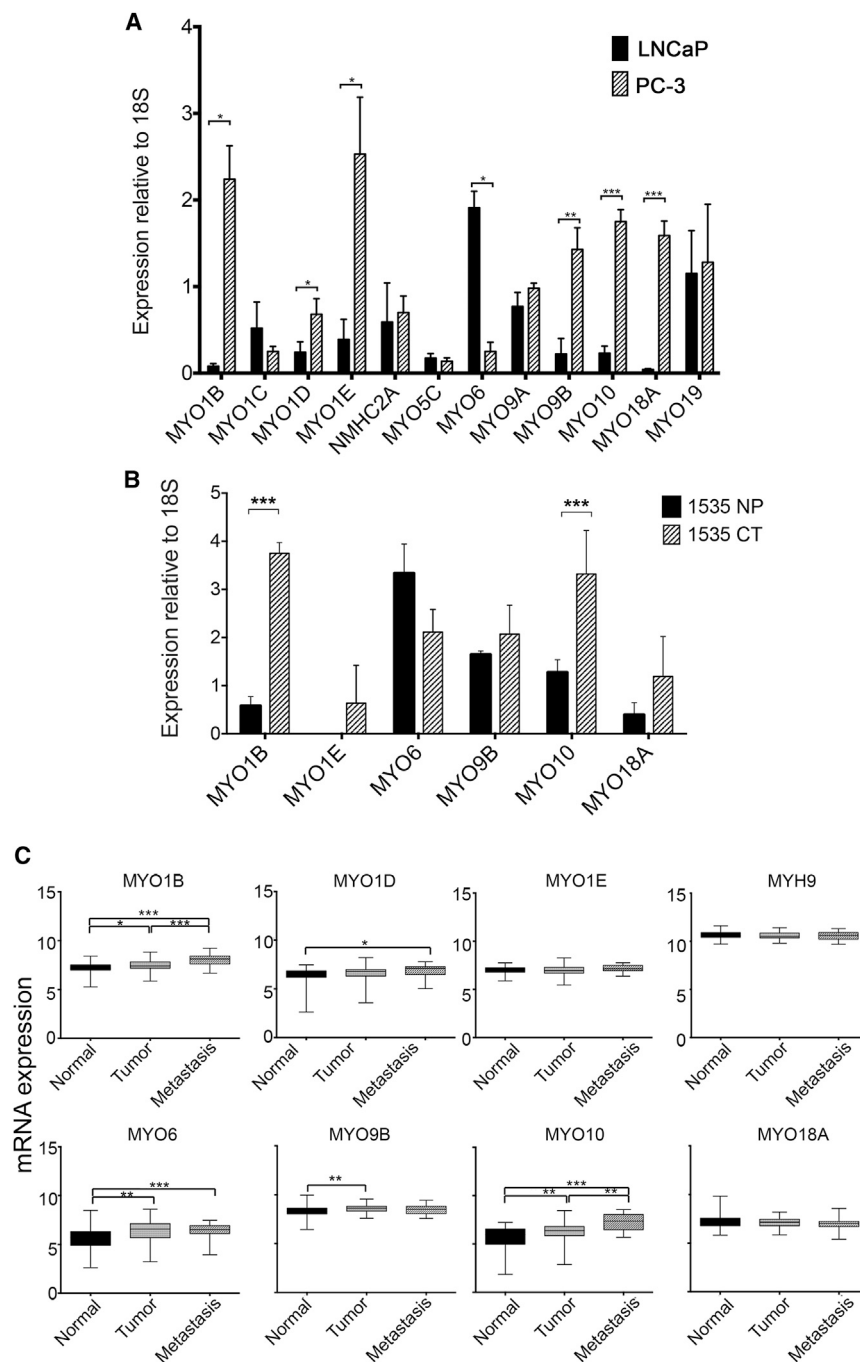
CrossMark

Figure 1. Myosin Expression Profiles in Tumors and Prostate Cancer Cell Lines

(A) Comparison of the expression levels for 12 of the myosin isoforms expressed by LNCaP and PC-3 cells, detected by qPCR. Data are presented as mean ± SD (n = 3).

(B) Comparison of the expression levels for six myosin isoforms expressed by a pair of matched (normal [1535NP] and cancerous [1535CT]) prostate cancer cell lines, detected by qPCR. Data are presented as mean ± SD (n = 3).

(C) In silico analysis of the mRNA expression levels for eight myosin isoforms in 171 (GEO: GSE6919) prostate tumor samples. Data are shown as the log2 expression ratio. Clinical tumor classification and number of samples are indicated.

$*p < 0.05$, $**p < 0.01$, $***p < 0.001$.

1535CT than in 1535NP cells (Figure 1B), and highest in localized medium-grade tumors (Figure 1C), as reported earlier (Dunn et al., 2006; Puri et al., 2010). *MYO9B* expression levels were increased in tumors compared with benign tissues (Figure 1C). Levels of *MYH9*, the only non-muscle myosin 2 gene we found to be expressed in prostate cancer cells, did not change at the mRNA level (Figure 1A) between LNCaP and PC-3 cells or between normal, tumor, or metastatic samples in the in silico analysis. Western blotting for Myo1b, NM2A, Myo6, Myo9b, Myo10, Myo18a, and NM2A in PC-3 and LNCaP cells (Figures 2A and 2B) showed similar trends in protein expression levels.

In PC-3 cells, high endogenous levels of Myo10 were associated with a high number of filopodia (Figures 2C and 2D), in which Myo10 was localized to the tips (Figure 2F), as expected from its known role in filopodium formation (Berg and Cheney, 2002; Berg et al., 2000). In contrast, both filopodium number and Myo10 expression levels were low in LNCaP cells (Figure 2C), staining was diffuse, and Myo10 was often absent from filopodial tips (Figures 2E and 2F). Upregulation of Myo10 in breast cancer cells has been linked to expression of mutant p53 (Arjonen et al., 2014). However, LNCaP cells are p53 wild-type, and PC-3 cells are p53-null (Carroll et al., 1993), suggesting that, in this case, there is no link between Myo10 overexpression and expression of mutant p53. In DU145 cells, which do express mutant p53, Myo10 expression is slightly higher, and numbers of filopodia are increased compared with LNCaP cells (Figures S1A and S1B), but both are lower compared with PC-3 cells.

Myo1b localized to organelles in both cell types (Figures 2D and 2E), as expected from its roles in trafficking of endosomes,

MYO1D, and *MYO10* levels were significantly higher in metastatic tumors than in benign tissue, suggesting that this trend is also found in vivo. *MYO1E* and *MYO18A* expression levels were also higher in 1535CT cells compared with 1535NP cells, although this difference was not significant, and the in silico analysis did not show any significant differences in expression (Figure 1C). However, the expression of *MYO18A* or *MYO1E* may be upregulated in some tumors. *MYO6* expression levels were significantly lower in PC-3 cells compared with LNCaP (Figure 1A), lower in
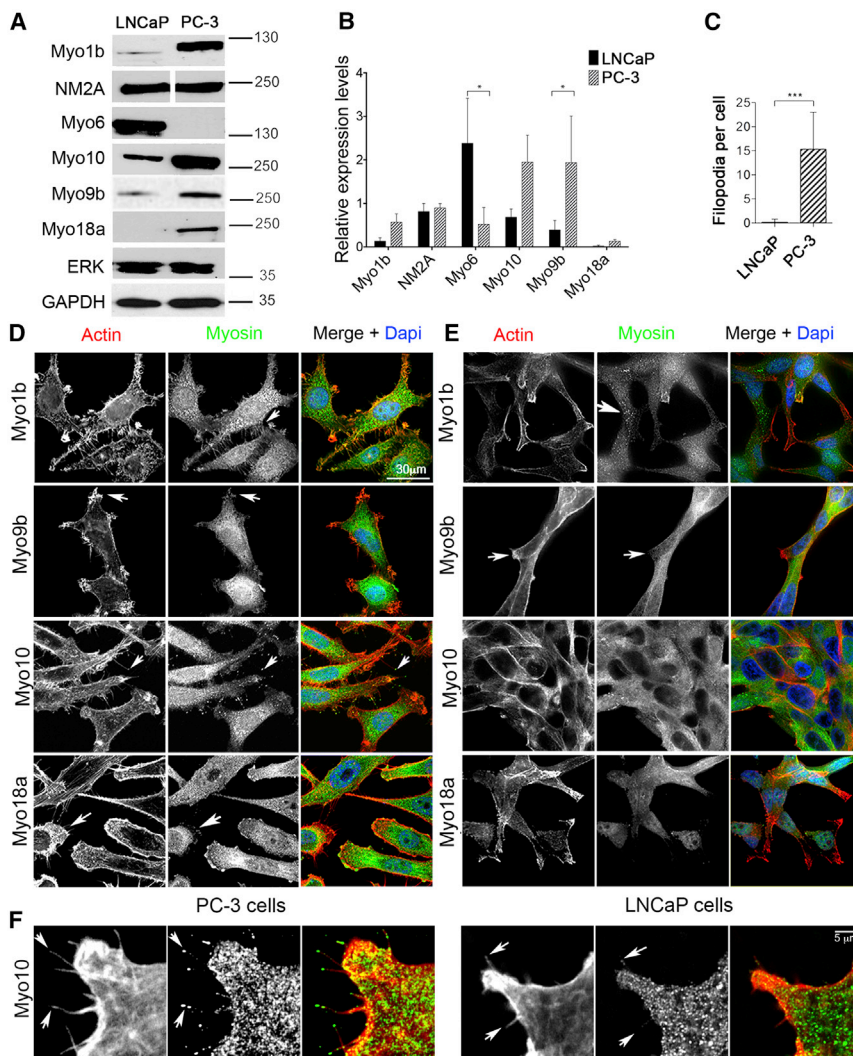
Figure 2. Expression and Localization of Myosin Isoforms in LNCaP and PC-3 Cells

(A and B) Example immunoblots (A) showing the variation in expression levels for five myosin isoforms in PC-3 and LNCaP cells. Molecular markers (in kilodalton) are shown on the right. Anti-Myo18a shows a single band with a molecular weight close to 230 kDa, suggesting that only the α isoform is expressed (Mori et al., 2003). The results are quantified in (B). Data are presented as mean ± SD (n = 3). Expression levels were compared with total p44/p42 MAPK (ERK) for all isoforms except Myo9b, for which GAPDH was used. GAPDH gave similar results as ERK as a loading control.

(C) Quantification of numbers of filopodia in LNCaP and PC-3 cells (n = 20).

(D and E) Maximum intensity projection images for PC-3 (D) and LNCaP (E) cells immunostained for F-actin (red) and either Myo1b, Myo9b, Myo10, or Myo18a (green). The arrows in (D) indicate Myo1b localization within filopodia, Myo9b in actin rich protrusions, Myo10 at filopodial tips, and Myo18 in actin-rich lamellae. The arrows in (E) indicate Myo1b localization to vesicles and lack of Myo9b in actin-rich protrusions. Merged images include nuclear staining using DAPI (blue). Scale bar, 30 μm.

(F) Many filopodia, and Myo10 at their tips PC-3 cells, contrasted with few filopodia with lack of Myo10 localization in LNCaP cells.

*p < 0.05, **p < 0.01, ***p < 0.001.

Knockdown of Myo1b, Myo9b, Myo10, and Myo18a Results in Isoform-Specific Changes in Cell Morphology, Cell Migration, and Actin Bundle Organization in PC-3 Cells

siRNA-mediated KD for 72 hr significantly reduced expression levels of each myosin isoform in PC-3 cells (Figure 3A) and altered their morphology (Figure 3B). The spread area of the cells increased up to 3-fold (Figure 3C). KD of Myo10, but not Myo1b, Myo9b, or Myo18a, also significantly reduced the numbers of filopodia (Figure 3D). Although the increase in cell area in Myo10 KD cells could be explained by the reduction in filopodia, as reported for COS-7 and HeLa cells (Bohil et al., 2006), it does not explain the increased cell area for Myo1b, Myo9b, and Myo18a KD cells, where filopodia are still present.

Myo9b and Myo10 were most important for PC-3 cell migration in 2D. Knockdown of Myo9b and Myo10 both significantly reduced cell speed ~2-fold in a 2D random migration assay (Figures 3E and 3F). Directional persistence was increased slightly for Myo9b KD cells but unaltered for Myo10. In contrast, knockdown of Myo1b and Myo18a did not affect speed in 2D random migration assays (Figures 3E and 3F). Knockdown of Myo18a significantly reduced directional persistence in 2D (Figures 3E and 3G), indicating that these cells are less able to polarize. However, cell migration was inhibited for each myosin in a circular invasion assay (Figure 3H) that closely mimics 3D invasion (Yu and Machesky, 2012). Staining for F-actin in circular migration

multivesicular bodies, and lysosomes (Cordonnier et al., 2001; Raposo et al., 1999; Salas-Cortes et al., 2005). Higher Myo1b expression in PC-3 cells was associated with an additional localization of Myo1b to actin-rich structures at the plasma membrane and filopodia (Figure 2D), consistent with an earlier study (Tang and Ostap, 2001). Myo9b and Myo18a were both enriched in membrane ruffles/lamellipodia in PC-3 cells (Figure 2D), consistent with Myo18a's role in modifying actin organization in the lamellipodium (Hsu et al., 2010) and Myo9b's role in cell polarity and recruitment of RhoGAP to the lamellipodium (Hanley et al., 2010). Staining for both was diffuse in LNCaP cells.

The higher endogenous expression levels of Myo1b, Myo9b, and Myo10 in more metastatic cell types/tissue suggested that they all contribute to the cellular phenotype of metastatic cells. We therefore used siRNA knockdown (KD) to determine the effects of reducing their expression levels in PC-3 cells on cell morphology and cell migration. We also investigated Myo18a because the interaction of Myo18a regulates NM2A filaments (Billington et al., 2015) and, therefore, may also influence cell migration and phenotype.
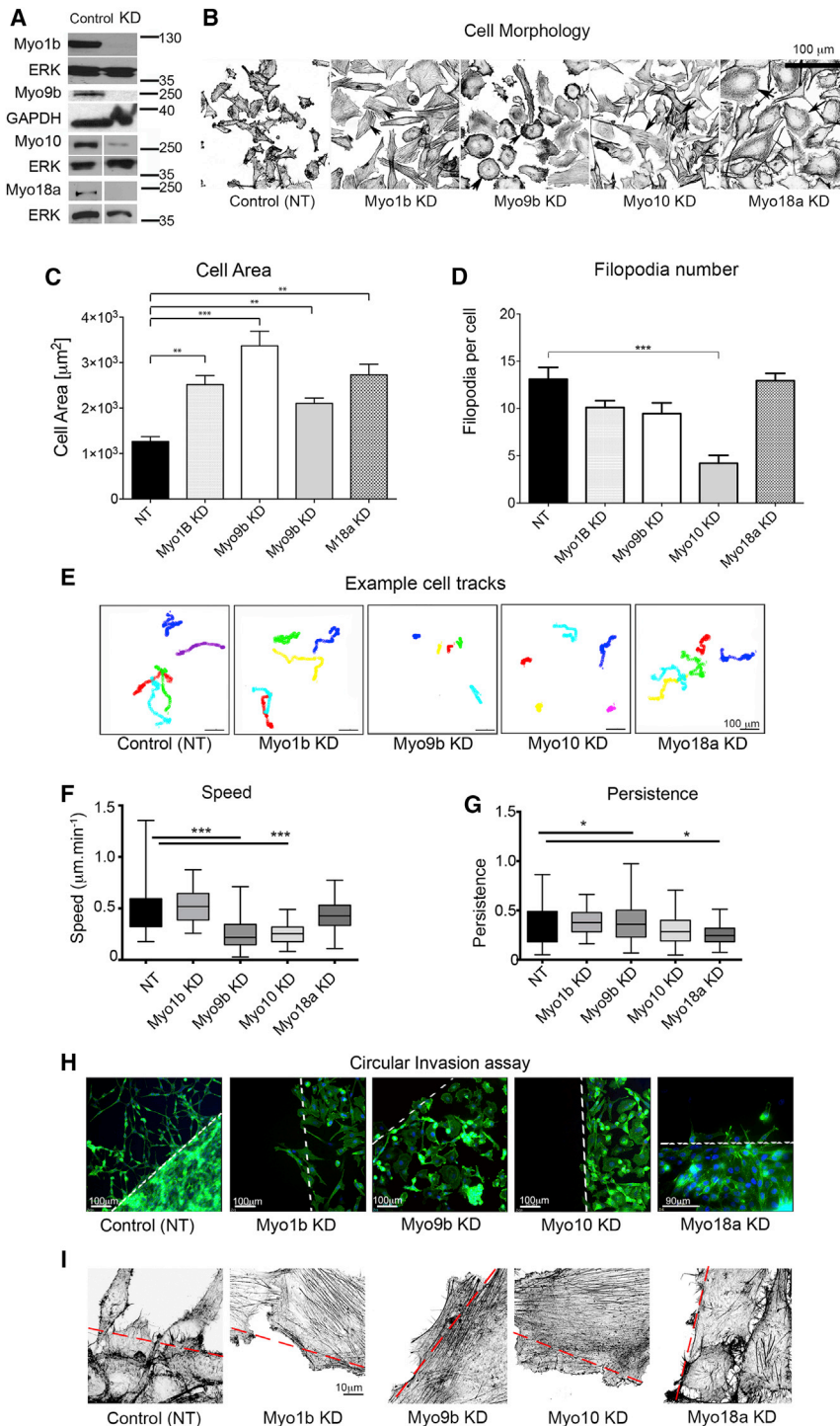
A Control KD

Myo1b ─130
ERK ─35
Myo9b ─250
GAPDH ─40
Myo10 ─250
ERK ─35
Myo18a ─250
ERK ─35

B Cell Morphology
100 μm

Control (NT)   Myo1b KD   Myo9b KD   Myo10 KD   Myo18a KD

C Cell Area

D Filopodia number

E Example cell tracks

Control (NT)   Myo1b KD   Myo9b KD   Myo10 KD   Myo18a KD
100 μm

F Speed

G Persistence

H Circular Invasion assay

Control (NT)   Myo1b KD   Myo9b KD   Myo10 KD   Myo18a KD

I

Control (NT)   Myo1b KD   Myo9b KD   Myo10 KD   Myo18a KD

Figure 3. Knockdown of Myosin 1b, 9b, 10, and 18a Affects Morphology and Cell Migration of PC-3 Cells

(A) KD of Myo1b, Myo9b, Myo10, or Myo18a in PC-3 cells analyzed by immunoblotting after 72 hr confirms that myosin levels are reduced significantly. Loading control: total ERK or GAPDH.

(B) Representative fields showing control and myosin-depleted PC-3 cells stained for F-actin using fluorescent phalloidin, obtained by tiling using the ×40 objective on the Zeiss LSM 880. Images are shown in reverse contrast. Arrowheads show prominent stress fibers (Myo1b KD), peripheral high-density actin staining (Myo9b KD), central stress fiber bundles (Myo10 KD), and increased actin in lamellae (Myo18a KD).

(C and D) Quantification of cell area (C) and number of filopodia (D) in control and myosin KD cells (n = 20). NT, control cells treated with non-targeting siRNA.

(E) Representative tracks for individual cells during an overnight time-lapse microscopy experiment for control (treated with non-targeting siRNA) and Myo1b, Myo9b, Myo10, and Myo18a-KD cells after HGF stimulation. Each colored line represents the track taken by an individual cell in the field.

(F and G) Quantification of speed (F) and directional persistence (G) of cell migration (n = 50 cells). Data were plotted as box-and-whisker plots, with whiskers showing maximum and minimum values.

(H) Circular invasion assay showing cells stained for F-actin and nuclei (DAPI). The dashed line marks the border of cell-free space that was created by stoppers before their removal. Scale bar, 100 μm and 90 μm (Myo18a KD).

(I) Magnified images of cells at the border of the cell-free space stained for F-actin. Scale bar, 10 μm.

$*p < 0.05$, $**p < 0.01$, $***p < 0.001$.

NM2A staining was mostly localized to the lamellae. A marked increase in centripetal F-actin fibers running parallel to the plasma membrane in the lamella associated with NM2A filaments was characteristic of Myo18a KD (Figures 4A and 4B). The appearance of sparse, long stress fibers, associated with NM2A and extended along the length of the cells, was characteristic of Myo1b KD (Figures 4A–4C). A line profile analysis of the frequency of actin bundles in the lamellae of KD cells showed that the frequency of bundles was reduced significantly (2.1 ± 0.1 bundles/μm, mean ± SEM, n = 9) compared with controls (2.6 ± 0.2 bundles/μm, mean ± SEM, n = 9, p < 0.5%) (Figures 4A and 4B), suggesting that the actin cytoskeleton is being reorganized. Myo9b KD cells contained a distinctive actin-rich area at the cell periphery from which NM2A was largely absent, in addition to an increase in stress fibers (Figures 4A and 4B).
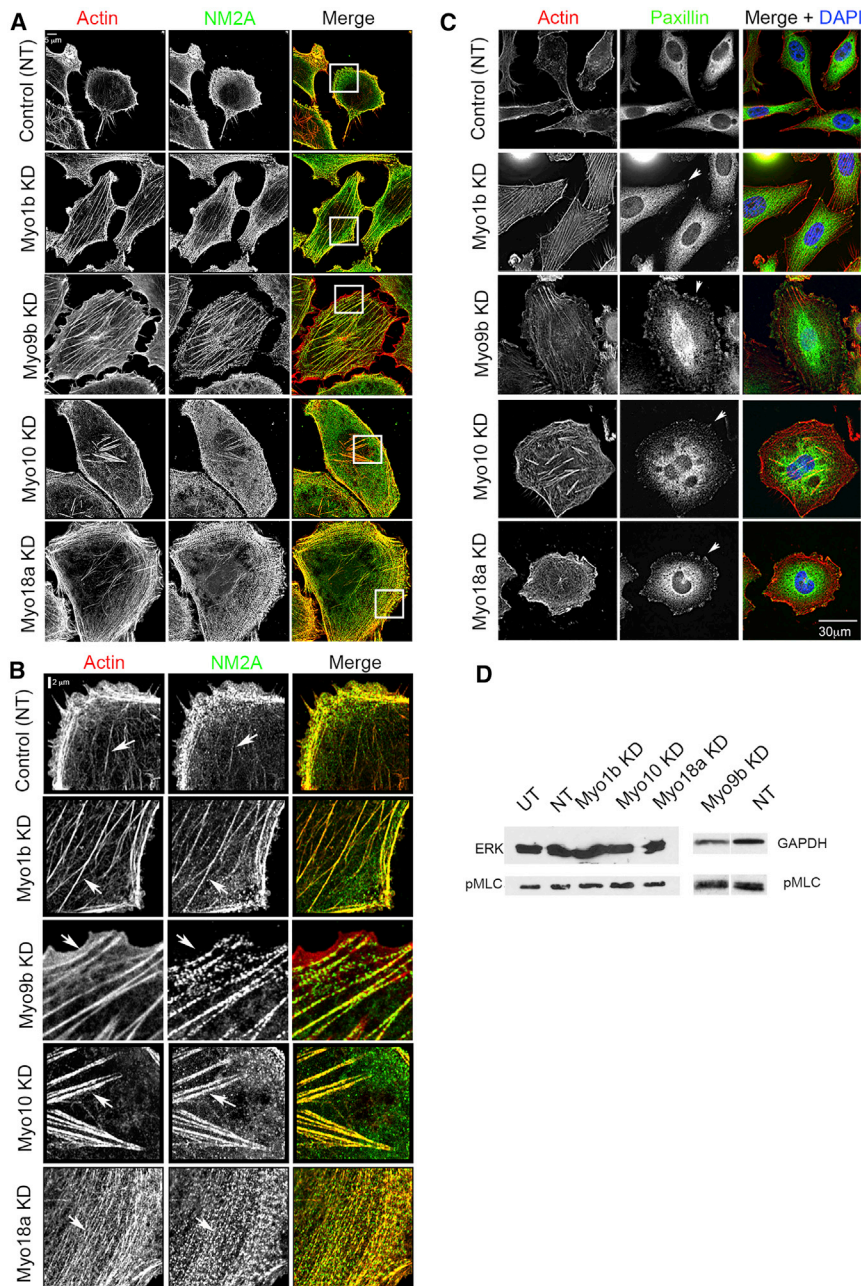
assays (Figure 3I) showed an increase in actin stress fibers for cells at the border for each myosin knockdown compared with controls.

We also observed distinct changes in the acto-myosin organization following KD of each myosin. Control PC-3 cells (Figures 4A and 4B) contained few F-actin stress fibers, and

Figure 4. Knockdown of Myosin 1b, 9b, 10, and 18a Affects Focal Adhesion and Actin and NM2A Organization in PC-3 Cells

(A and B) Control cells treated with non-targeting siRNA and myosin-depleted cells co-stained for F-actin (red) and NM2A (green) (A). An enlarged view of the region in the boxed area in (A) is shown in (B). Arrowheads indicate F-actin structures in KD cells. Scale bars, 5 μm (A) and 2 μm (B).

(C) Control NT cells and myosin-depleted cells co-stained for F-actin (red) and focal adhesions using paxillin (green). Arrowheads indicate focal adhesions at the ends of F-actin bundles in KD cells Scale bar, 30 μm.

(D) Immunoblotting for phosphorylated myosin light chain (pMLC) and ERK or GAPDH (loading control) in control and KD cells. Quantification of the control and Myo9b KD blot shown here showed a 1.8-fold increase in pMLC in KD compared with NT cells. UT, untreated.

DISCUSSION

These data show that Myo10, Myo9b, and Myo1b are overexpressed in more highly metastatic cell lines and in metastatic tissue. High levels of Myo10 in PC-3 cells are linked to high numbers of filopodia, and high levels of Myo9b are linked to low levels of stress fibers. Both isoforms contribute to a more migratory phenotype, as shown by immunostaining, cell migration, and KD experiments. Myo1b and Myo18a influence cell morphology and actin organization but have little effect on migration in 2D, whereas all four isoforms inhibit cell migration in invasion assays. Therefore, changes in expression of several myosin isoforms may contribute to metastasis in prostate cancer.

Our finding that Myo10-dependent filopodia are likely to be important in prostate cancer agrees with recent similar findings for breast cancer metastasis (Arjonen et al., 2014; Cao et al., 2014) and non-small lung cell cancer (Sun et al., 2015). Filopodia are important but not

Myo10 KD cells showed loss of filopodia and the appearance of distinctive actin bundles in the central region of the cell (Figures 4A and 4B).

Changes to the F-actin organization were associated with formation of focal adhesions at the edges of the cells, consistent with a more spread cell phenotype (Figure 4C). Knockdown of Myo1b, Myo10, or Myo18a did not change phosphorylation levels of myosin light chain (MLC) (Figure 4D), suggesting that NM2A is re-organized rather than activated as a result of their knockdown. Myo9b KD did increase MLC phosphorylation ~2-fold in cells, and this is likely to contribute to the actomyosin re-organization observed (Figure 4D).

absolutely required for cell migration because Myo10 KD cells can migrate in 2D but with a reduced speed, and other cells lacking filopodia can migrate (Lundquist, 2009). The increased cell area resulting from Myo10 KD agrees with previous findings (Bohil et al., 2006). The central actin bundles in Myo10 knockdown cells are reminiscent of actin bundles in filopodia. Fascin is also required for filopodial formation (Vignjevic et al., 2006), its overexpression results in multiple filopodia (Vignjevic et al., 2006), and fascin levels are also upregulated in prostate cancer (Darnel et al., 2009). Myo10 KD may lead to actin bundling in the cell body by excess (non-phosphorylated) fascin. The role of two filopodial proteins, Myo10 and fascin, in prostate (and other)

cancers suggest that filopodium formation is key for metastasis. Myo10 has also been implicated in integrin-mediated adhesion, and any reduction in adhesion resulting from its KD could disrupt signaling to the actin cytoskeleton and, therefore, indirectly result in changes in actin organization.

High levels of Myo9b expression in PC-3 cells are likely to contribute to their lack of stress fibers and, therefore, to enhanced migration. The RhoGTPase-activating domain in Myo9b inhibits Rho, reducing the downstream activity of ROCK (RhoKinase), thereby increasing MLC phosphatase activity, reducing MLC phosphorylation (Reinhard et al., 1995; Wirth et al., 1996), and, therefore, reducing actin stress fiber formation. Knockdown of Myo9b is therefore expected to increase MLC phosphorylation and stress fiber formation, as we observed. In agreement with our findings, a previous report has shown that cell migration was reduced and MLC phosphorylation increased in macrophages isolated from Myo9b knockout mice (Hanley et al., 2010). Myo9b has also been implicated in an increased risk of esophageal cancer (Menke et al., 2012).

The high levels of Myo1b in PC-3 cells and effects of knockdown on 3D invasion, cell shape, and morphology suggest that it, too, has a role in prostate cancer. Myo1b has also been implicated in non-small-cell lung cancers (Ohmura et al., 2015). Myo1b (Myr1/MM1α; Gillespie et al., 2001) regulates actin assembly in vesicular transport (post-Golgi carriers [Almeida et al., 2011] and endocytic organelles [Cordonnier et al., 2001; Raposo et al., 1999]), and it maintains cortical tension at the plasma membrane, where it specifically associates with dynamic, non-tropomyosin-containing actin filaments (Coluccio and Geeves, 1999; Tang and Ostap, 2001). High endogenous levels of Myo1b in more highly metastatic cells might therefore increase cortical tension, allowing cells to move through stiff extracellular matrices in vivo, perhaps explaining why knockdown of Myo1b only affects migration in 3D but not 2D.

Myo18a could contribute to metastasis in prostate cancer. The re-organization of actin and NM2A in Myo18a KD cells may arise from its interaction with non-muscle myosin 2 (NM2). NM2 forms short filaments (~300 nm long) containing ~20 molecules (Billington et al., 2013). The assembly/disassembly of non-muscle myosin 2 filaments is dynamic (Shutova et al., 2014) and regulated by many different pathways (Vicente-Manzanares et al., 2009). Myo18a and NM2A can form mixed bipolar filaments in vitro that are smaller that pure NM2A filaments (Billington et al., 2015). The re-organization of NM2A we observed after knocking down Myo18a, without a change to levels of light chain phosphorylation, supports the idea that an interaction between Myo18a and NM2A modulates NM2A filament formation and organization in PC-3 cells.

Therefore, Myo1b, Myo9b, Myo10, and Myo18a each contribute to the morphology and migration of more highly metastatic PC-3 cells, with each myosin having a specific effect on actin organization. Misregulation of their expression in cells with metastatic potential may allow them to work in concert to generate a torpedo-shaped cell with multiple protrusions that is better able to migrate through a 3D matrix and, therefore, more able to metastasize. Many different drugs have now been developed that can inhibit specific myosin isoforms, including those in classes 1, 2, 5, and 6 (Bond et al., 2013). Developing drugs to block specific myosin functions could be useful in preventing metastasis. Importantly, these results emphasize that myosin not only uses actin as tracks to walk along but that it is able to actively drive actin organization in cells.

EXPERIMENTAL PROCEDURES

Cell Culture

LNCaP, DU145, and PC-3 cells (from the ATCC) were grown in RPMI 1640 medium with GlutaMAX (Gibco, Life Technologies) supplemented with 10% heat-inactivated fetal bovine serum (FBS) and penicillin-streptomycin. 1535NP and CT cells (Bright et al., 1997) were a gift from Suzanne Topalian (Johns Hopkins University School of Medicine). They were grown in keratinocyte medium (Gibco, Life Technologies) supplemented with 10% heat-inactivated FBS, 1% L-glutamine, antibiotics, bovine pituitary extract, and epidermal growth factor.

Antibodies and Reagents

The antibodies used were as follows: Myo6 (H-215, Santa Cruz Biotechnology); Myo10 (HPA024223, Sigma); total ERK (p44/42 mitogen-activated protein kinase [MAPK], Cell Signaling Technology); Myo18a, a gift from Prof. Yu and Dr. Hsu (Chang Gung University, Taiwan; Hsu et al., 2010) or from Genscript; NM2A (PRB-440P, Covance); paxillin (SAB4502553, Sigma); Myo1b (HPA013607, Sigma); phospho-myosin light chain (Cell Signal); Myo9b (Proteintech); and glyceraldehyde 3-phosphate dehydrogenase (GAPDH) (Abcam). HRP-conjugated secondary antibodies and fluorescent phalloidin were from Sigma, and fluorescent secondary antibodies were from Molecular Probes.

Transfections

siGENOME SMARTpool siRNA (GE Healthcare, Dharmacon) was used to silence myosins in PC-3 cells. Cells were seeded at a density of 20,000 cells/ml in growth media and allowed to adhere and grow overnight. Lipofectamine RNAiMAX reagent (Invitrogen, Life Technologies) was used for transfections. Maximum KD was achieved after 72 hr.

PCR

The RNeasy mini kit (QIAGEN) was used to extract cellular RNA. cDNA was synthesized using avian myeloblastosis virus (AMV) reverse transcriptase. RT-PCR was used to detect which myosin isoforms were expressed (Table S1). Real-time PCR using SYBR Green was used to investigate the expression levels of expressed myosins (see Table S2 for primer sequences). Data analysis was performed using a Bio-Rad system and software.

Immunoblotting

Cells were lysed (30 min, 4°C) in lysis buffer (150 mM NaCl, 0.05 M Tris [pH 8], 1% Triton X-100, and 1 mM EDTA [pH 8] with protease inhibitor cocktail (Thermo Scientific). Lysates were clarified by centrifugation, protein content was quantified by bicinchoninic acid (BCA) assay, and then samples were mixed with 2× Laemmli buffer for use in protein gels (4%–20% or 7.5%) and blots. Chemiluminescence detection (Supersignal West Pico, Thermo Scientific) used multiple exposures to ensure signal linearity. If required, membranes were stripped using Restore western blot stripping buffer (Thermo Scientific) and re-probed.

Immunostaining

Cells were grown on glass coverslips, fixed with 2% paraformaldehyde in PBS, and stained using standard procedures (Swailes et al., 2006). Cells were imaged using a DeltaVision deconvolution microscope or Zeiss880 Airyscan.

Migration Assays

For 2D assays, cells were plated onto a glass-bottomed 96-well plates, transfected with non-targeting siRNA or with myosin KD siRNA (three replicates each), serum-starved 48 hr later for 24 hr, and then treated with hepatocyte growth factor (HGF) (25 ng/ml) for filming. A minimum of three fields from each replicate was selected for imaging, over 14 hr at 5-min intervals using

differential interference contrast (DIC) optics, and a 20× lens (512 × 512 total pixel size, 2 × 2 binning) on a DeltaVision system. Cell migration was analyzed using ImageJ software (MTrackJ plugin). To perform the 3D-like circular invasion assay (Yu and Machesky, 2012), cell-free space was created using cell stoppers (Ibidi). After removing the stopper, cells were covered with a thin layer of Matrigel (4 mg/ml) and normal medium and allowed to grow and migrate for another 24–48 hr. Cells were then fixed in 2% paraformaldehyde (PFA) and stained.

Data Analysis

Immunoblots and digitized images of immunostained cells were analyzed using ImageJ. GraphPad Prism 5.0 was used to analyze data. Data are presented as mean ± SD for at least three separate experiments (n ≥ 3). A two-way ANOVA was used to compare differences between groups, and statistical significance was accepted for $p \leq 0.05$.

SUPPLEMENTAL INFORMATION

AUTHOR CONTRIBUTIONS

Conceptualization, C.M.W. and M.P.; Methodology, K.A.M., C.M.W., and M.P.; Investigation, K.A.M., K.J.W., R.H., and M.P.; Writing – Original Draft, K.A.M. and M.P.; Writing – Review & Editing, K.A.M., C.M.W., and M.P.; Funding Acquisition, C.M.W. and M.P.; Resources, C.M.W. and M.P.; Supervision, C.M.W. and M.P.

ACKNOWLEDGMENTS

REFERENCES

Aalinkeel, R., Nair, M.P., Sufrin, G., Mahajan, S.D., Chadha, K.C., Chawda, R.P., and Schwartz, S.A. (2004). Gene expression of angiogenic factors correlates with metastatic potential of prostate cancer cells. Cancer Res. 64, 5311–5321.

Almeida, C.G., Yamada, A., Tenza, D., Louvard, D., Raposo, G., and Coudrier, E. (2011). Myosin 1b promotes the formation of post-Golgi carriers by regulating actin assembly and membrane remodelling at the trans-Golgi network. Nat. Cell Biol. 13, 779–789.

Arjonen, A., Kaukonen, R., Mattila, E., Rouhi, P., Högnäs, G., Sihto, H., Miller, B.W., Morton, J.P., Bucher, E., Taimen, P., et al. (2014). Mutant p53-associated myosin-X upregulation promotes breast cancer invasion and metastasis. J. Clin. Invest. 124, 1069–1082.

Bement, W.M., Hasson, T., Wirth, J.A., Cheney, R.E., and Mooseker, M.S. (1994). Identification and overlapping expression of multiple unconventional myosin genes in vertebrate cell types. Proc. Natl. Acad. Sci. USA 91, 11767.

Berg, J.S., and Cheney, R.E. (2002). Myosin-X is an unconventional myosin that undergoes intrafilopodial motility. Nat. Cell Biol. 4, 246–250.

Berg, J.S., Derfler, B.H., Pennisi, C.M., Corey, D.P., and Cheney, R.E. (2000). Myosin-X, a novel myosin with pleckstrin homology domains, associates with regions of dynamic actin. J. Cell Sci. 113, 3439–3451.

Berg, J.S., Powell, B.C., and Cheney, R.E. (2001). A millennial myosin census. Mol. Biol. Cell 12, 780–794.

Billington, N., Wang, A., Mao, J., Adelstein, R.S., and Sellers, J.R. (2013). Characterization of three full-length human nonmuscle myosin II paralogs. J. Biol. Chem. 288, 33398–33410.

Billington, N., Beach, J.R., Heissler, S.M., Remmert, K., Guzik-Lendrum, S., Nagy, A., Takagi, Y., Shao, L., Li, D., Yang, Y., et al. (2015). Myosin 18A coassembles with nonmuscle myosin 2 to form mixed bipolar filaments. Curr. Biol. 25, 942–948.

Bohil, A.B., Robertson, B.W., and Cheney, R.E. (2006). Myosin-X is a molecular motor that functions in filopodia formation. Proc. Natl. Acad. Sci. USA 103, 12411–12416.

Bond, L.M., Tumbarello, D.A., Kendrick-Jones, J., and Buss, F. (2013). Small-molecule inhibitors of myosin proteins. Future Med. Chem. 5, 41–52.

Bright, R.K., Vocke, C.D., Emmert-Buck, M.R., Duray, P.H., Solomon, D., Fetsch, P., Rhim, J.S., Linehan, W.M., and Topalian, S.L. (1997). Generation and genetic characterization of immortal human prostate epithelial cell lines derived from primary cancer specimens. Cancer Res. 57, 995–1002.

Cao, R., Chen, J., Zhang, X., Zhai, Y., Qing, X., Xing, W., Zhang, L., Malik, Y.S., Yu, H., and Zhu, X. (2014). Elevated expression of myosin X in tumours contributes to breast cancer aggressiveness and metastasis. Br. J. Cancer 111, 539–550.

Carroll, A.G., Voeller, H.J., Sugars, L., and Gelmann, E.P. (1993). p53 oncogene mutations in three human prostate cancer cell lines. Prostate 23, 123–134.

Coluccio, L.M., and Geeves, M.A. (1999). Transient kinetic analysis of the 130-kDa myosin I (MYR-1 gene product) from rat liver. A myosin I designed for maintenance of tension? J. Biol. Chem. 274, 21575–21580.

Cordonnier, M.N., Dauzonne, D., Louvard, D., and Coudrier, E. (2001). Actin filaments and myosin I alpha cooperate with microtubules for the movement of lysosomes. Mol. Biol. Cell 12, 4013–4029.

Darnel, A.D., Behmoaram, E., Vollmer, R.T., Corcos, J., Bijian, K., Sircar, K., Su, J., Jiao, J., Alaoui-Jamali, M.A., and Bismar, T.A. (2009). Fascin regulates prostate cancer cell invasion and is associated with metastasis and biochemical failure in prostate cancer. Clin. Cancer Res. 15, 1376–1383.

Dosé, A.C., and Burnside, B. (2000). Cloning and chromosomal localization of a human class III myosin. Genomics 67, 333–342.

Dunn, T.A., Chen, S., Faith, D.A., Hicks, J.L., Platz, E.A., Chen, Y., Ewing, C.M., Sauvageot, J., Isaacs, W.B., De Marzo, A.M., and Luo, J. (2006). A novel role of myosin VI in human prostate cancer. Am. J. Pathol. 169, 1843–1854.

Gillespie, P.G., Albanesi, J.P., Bahler, M., Bement, W.M., Berg, J.S., Burgess, D.R., Burnside, B., Cheney, R.E., Corey, D.P., Coudrier, E., et al. (2001). Myosin-I nomenclature. J. Cell Biol. 155, 703–704.

Hanley, P.J., Xu, Y., Kronlage, M., Grobe, K., Schön, P., Song, J., Sorokin, L., Schwab, A., and Bähler, M. (2010). Motorized RhoGAP myosin IXb (Myo9b) controls cell shape and motility. Proc. Natl. Acad. Sci. USA 107, 12145–12150.

Hartman, M.A., and Spudich, J.A. (2012). The myosin superfamily at a glance. J. Cell Sci. 125, 1627–1632.

Hasson, T., Heintzelman, M.B., Santos-Sacchi, J., Corey, D.P., and Mooseker, M.S. (1995). Expression in cochlea and retina of myosin VIIa, the gene product defective in Usher syndrome type 1B. Proc. Natl. Acad. Sci. USA 92, 9815–9819.

Hsu, R.M., Tsai, M.H., Hsieh, Y.J., Lyu, P.C., and Yu, J.S. (2010). Identification of MYO18A as a novel interacting partner of the PAK2/betaPIX/GIT1 complex and its potential function in modulating epithelial cell migration. Mol. Biol. Cell 21, 287–301.

Lundquist, E.A. (2009). The finer points of filopodia. PLoS Biol. 7, e1000142.

Menke, V., Van Zoest, K.P., Moons, L.M., Pot, R.G., Siersema, P.D., Kuipers, E.J., and Kusters, J.G. (2012). Myo9B is associated with an increased risk of Barrett's esophagus and esophageal adenocarcinoma. Scand. J. Gastroenterol. 47, 1422–1428.

Mogilner, A., and Keren, K. (2009). The shape of motile cells. Curr. Biol. 19, R762–R771.

Mori, K., Furusawa, T., Okubo, T., Inoue, T., Ikawa, S., Yanai, N., Mori, K.J., and Obinata, M. (2003). Genome structure and differential expression of two isoforms of a novel PDZ-containing myosin (MysPDZ) (Myo18A). J. Biochem. *133*, 405–413.

Ohmura, G., Tsujikawa, T., Yaguchi, T., Kawamura, N., Mikami, S., Sugiyama, J., Nakamura, K., Kobayashi, A., Iwata, T., Nakano, H., et al. (2015). Aberrant Myosin 1b Expression Promotes Cell Migration and Lymph Node Metastasis of HNSCC. Mol. Cancer Res. *13*, 721–731.

Peckham, M., and Knight, P. (2009). When a predicted coiled coil is really a single α-helix, in myosins and other proteins. Soft Matter *5*, 2493–2503.

Pulukuri, S.M., Gondi, C.S., Lakka, S.S., Jutla, A., Estes, N., Gujrati, M., and Rao, J.S. (2005). RNA interference-directed knockdown of urokinase plasminogen activator and urokinase plasminogen activator receptor inhibits prostate cancer cell invasion, survival, and tumorigenicity in vivo. J. Biol. Chem. *280*, 36529–36540.

Puri, C., Chibalina, M.V., Arden, S.D., Kruppa, A.J., Kendrick-Jones, J., and Buss, F. (2010). Overexpression of myosin VI in prostate cancer cells enhances PSA and VEGF secretion, but has no effect on endocytosis. Oncogene *29*, 188–200.

Raposo, G., Cordonnier, M.N., Tenza, D., Menichi, B., Dürrbach, A., Louvard, D., and Coudrier, E. (1999). Association of myosin I alpha with endosomes and lysosomes in mammalian cells. Mol. Biol. Cell *10*, 1477–1494.

Reinhard, J., Scheel, A.A., Diekmann, D., Hall, A., Ruppert, C., and Bähler, M. (1995). A novel type of myosin implicated in signalling by rho family GTPases. EMBO J. *14*, 697–704.

Salas-Cortes, L., Ye, F., Tenza, D., Wilhelm, C., Theos, A., Louvard, D., Raposo, G., and Coudrier, E. (2005). Myosin Ib modulates the morphology and the protein transport within multi-vesicular sorting endosomes. J. Cell Sci. *118*, 4823–4832.

Shutova, M.S., Spessott, W.A., Giraudo, C.G., and Svitkina, T. (2014). Endogenous species of mammalian nonmuscle myosin IIA and IIB include activated monomers and heteropolymers. Curr. Biol. *24*, 1958–1968.

Sun, Y., Ai, X., Shen, S., and Lu, S. (2015). NF-κB-mediated miR-124 suppresses metastasis of non-small-cell lung cancer by targeting MYO10. Oncotarget *6*, 8244–8254.

Swailes, N.T., Colegrave, M., Knight, P.J., and Peckham, M. (2006). Non-muscle myosins 2A and 2B drive changes in cell morphology that occur as myoblasts align and fuse. J. Cell. Sci. *119*, 3561–3570.

Tang, N., and Ostap, E.M. (2001). Motor domain-dependent localization of myo1b (myr-1). Curr. Biol. *11*, 1131–1135.

Vicente-Manzanares, M., Ma, X., Adelstein, R.S., and Horwitz, A.R. (2009). Non-muscle myosin II takes centre stage in cell adhesion and migration. Nat. Rev. Mol. Cell Biol. *10*, 778–790.

Vignjevic, D., Kojima, S., Aratyn, Y., Danciu, O., Svitkina, T., and Borisy, G.G. (2006). Role of fascin in filopodial protrusion. J. Cell Biol. *174*, 863–875.

Weber, K.L., Sokac, A.M., Berg, J.S., Cheney, R.E., and Bement, W.M. (2004). A microtubule-binding myosin required for nuclear anchoring and spindle assembly. Nature *431*, 325–329.

Wells, C., Coles, D., Entwistle, A., and Peckham, M. (1997). Myogenic cells express multiple myosin isoforms. J. Muscle Res. Cell Motil. *18*, 501–515.

Wirth, J.A., Jensen, K.A., Post, P.L., Bement, W.M., and Mooseker, M.S. (1996). Human myosin-IXb, an unconventional myosin with a chimerin-like rho/rac GTPase-activating protein domain in its tail. J. Cell Sci. *109*, 653–661.

Yu, X., and Machesky, L.M. (2012). Cells assemble invadopodia-like structures and invade into matrigel in a matrix metalloprotease dependent manner in the circular invasion assay. PLoS ONE *7*, e30605.